Intensification of extratropical cyclones associated with the polar jet change in the CMIP5 global warming projections

Ryo Mizuta[1]

Received 8 July 2012; revised 28 August 2012; accepted 29 August 2012; published 3 October 2012.

[1] The projected change in intense extratropical cyclones in the Northern Hemisphere winter due to global warming is investigated using 11 climate models from the Coupled Model Intercomparison Project Phase 5 (CMIP5). In many models, the number of intense surface cyclones (sea-level pressure below 980 hPa) increases on the polar and downstream side of the storm tracks, and the mean growth rate of the cyclones is enhanced in areas upstream of these regions, especially in the North Pacific. Around these regions, the mean growth rate is highly correlated with the upper-level zonal wind on a monthly time scale, and its projected change can be largely explained by the zonal wind change. An enhanced polar jet over the North Pacific seen in many models leads to an enhanced mean growth rate of surface cyclones, while less agreement between the models is seen over the North Atlantic. **Citation:** Mizuta, R. (2012), Intensification of extratropical cyclones associated with the polar jet change in the CMIP5 global warming projections, *Geophys. Res. Lett.*, *39*, L19707, doi:10.1029/2012GL053032.

1. Introduction

[2] Changes in extratropical cyclone activity due to anthropogenic climate change projected in climate models have many variations depending on the metric of activity, as reviewed by *Ulbrich et al.* [2009]. Synoptic-scale activity (also called storm-track activity) is projected to increase in the middle-upper troposphere [*Yin*, 2005; *Ulbrich et al.*, 2008]. This change is consistent with the enhanced meridional temperature gradient in the upper troposphere. In contrast, the total number of surface cyclone tracks decreases in future climate experiments [*Geng and Sugi*, 2003; *Bengtsson et al.*, 2006]. This change is consistent with a weakened meridional temperature gradient near the surface. However, intense surface cyclones are projected to increase in many climate models [*Lambert and Fyfe*, 2006], which influences the occurrence of disasters in mid-latitudes through weather extremes such as extreme wind or heavy-precipitation events.

[3] *Mizuta et al.* [2011] have related the change in intense cyclones to changes in the middle-upper troposphere. Using a high-resolution AGCM and looking at the response to the sea-surface temperature (SST) change based on the multi-model ensemble mean, they found an increase in intense cyclones on the polar side and downstream side of Atlantic and Pacific storm tracks in the Northern Hemisphere winter, and enhancement of cyclone development in areas upstream of these regions. These regions correspond to regions with increasing zonal wind in the middle-upper troposphere. Although they used results of initial value ensemble experiments, uncertainty over future change remains, arising from systematic errors of the model in simulating the present climate. It is desirable to verify these results in multiple climate models.

[4] This study investigates how much of those results apply to the climate models from the Coupled Model Intercomparison Project Phase 5 (CMIP5) [*Taylor et al.*, 2012]. The CMIP5 models have more fine-scale output on both the spatial and temporal scales than those from Phase 3 (CMIP3) [*Meehl et al.*, 2007] and are sufficient to investigate these issues. Here, we focus on the Northern Hemisphere winter, from December to February (DJF).

2. Models and Methods

[5] The CMIP5 multi-model ensemble of simulations [*Taylor et al.*, 2012] is used. In this study, the differences from 1979–2003 in the Historical run (forced by observed atmospheric composition changes) and 2075–2099 in the RCP4.5 scenario run (forced by a midrange mitigation emissions scenario) are treated as projected changes induced by global warming. Therefore, among many climate models from many institutes, we use 11 CMIP5 models in which the six-hourly sea-level pressure (SLP), the daily zonal wind (U), and the daily meridional wind (V) are available for both periods. The models and the resolutions of their atmospheric parts are listed in Table 1. The Japanese 25-year Reanalysis (JRA-25 [*Onogi et al.*, 2007]; model resolution is 320 × 160 with 40 levels) is used to validate the Historical runs.

[6] The cyclone detection and tracking method used here is the same as that used in *Mizuta et al.* [2011], which is a modified version of the method by *Geng and Sugi* [2003]. It uses six-hourly SLP interpolated into a 1.25° grid: A point is identified as a candidate cyclone if its SLP is lower than any of the surrounding eight points and lower than the average of these eight points by 0.3 hPa (points with altitudes exceeding 1500 m are excluded). Next, each point is advected by the background flow (15-day running mean U and V at 700 hPa) for 6 hours. From the destination point, we search for the nearest point within 300 km at 6 hours later. If the point is found, the two related points are regarded as one sequence of a cyclone. Cyclones that persist for longer than 24 hours are analyzed in this study.

3. Results

[7] Figures 1a–1k show the density of intense cyclones simulated in the Historical run of each model. The density is

[1]Climate Research Department, Meteorological Research Institute, Tsukuba, Japan.

Corresponding author: R. Mizuta, Climate Research Department, Meteorological Research Institute, 1-1 Nagamine, Tsukuba, Ibaraki 305-0052, Japan. (rmizuta@mri-jma.go.jp)

0094-8276/12/2012GL053032

Table 1. Models Used in the Study and the Resolution (Longitude, Latitude, and Vertical) of Their Atmospheric Parts

Model Name	Institute (Country)	Resolution (Atmosphere)
BCC-CSM1.1	Beijing Climate Center, China Meteorological Administration (China)	128 × 64 × 26
CCSM4	National Center for Atmospheric Research (USA)	288 × 192 × 27
CSIRO-Mk3-6-0	Commonwealth Scientific and Industrial Research Organization and Bureau of Meteorology (Australia)	192 × 96 × 18
GFDL-ESM2G	NOAA Geophysical Fluid Dynamics Laboratory (USA)	144 × 90 × 24
HadGEM2-CC	Met Office Hadley Centre (UK)	192 × 145 × 60
INMCM4	Institute for Numerical Mathematics (Russia)	180 × 120 × 21
IPSL-CM5A-LR	Institut Pierre-Simon Laplace (France)	96 × 96 × 39
MIROC5	Atmosphere and Ocean Research Institute (The University of Tokyo), National Institute for Environmental Studies, and Japan Agency for Marine-Earth Science and Technology (Japan)	256 × 128 × 56
MPI-ESM-LR	Max Planck Institute for Meteorology (Germany)	192 × 96 × 47
MRI-CGCM3	Meteorological Research Institute (Japan)	320 × 160 × 48
NorESM1-M	Norwegian Climate Centre (Norway)	144 × 96 × 26

defined as the frequency of existence of cyclones that experience below 980 hPa during their lifetimes. The ensemble mean of all of the models is given in Figure 1l, and Figure 1m gives the corresponding data for the same period of JRA-25. In the reanalysis data, the density is high in 45°–60°N in the Pacific, with a local maximum slightly east of the dateline along the Aleutian Islands, and 50°–65°N in the Atlantic, with a local maximum between Greenland and Iceland. The geographical distribution is basically well simulated in each model, although the Pacific local maximum is slightly to the west in MPI-ESM-LR and to the east in MRI-CGCM3, and the Atlantic one is slightly southward in CSIRO-Mk3-6-0. The model dependence is larger from the quantitative point of view. The density is lower in a high-resolution model (MIROC5) and higher in other high-resolution models (CCSM4 and MRI-CGCM3), so it seems that the quantitative difference between the models are not from their resolutions (Table 1), but from other differences such as physical schemes. Overall, the ensemble mean of all of the models (Figure 1l) comes closer to the reanalysis (Figure 1m).

[8] Figure 2 shows the multi-model ensemble mean (MMEM) of the projected change and the agreement between the models on the sign of the change in the density of intense cyclones, the mean growth rate of cyclones, and the zonal wind at 500 hPa. The agreement value (Figures 2d–2f)

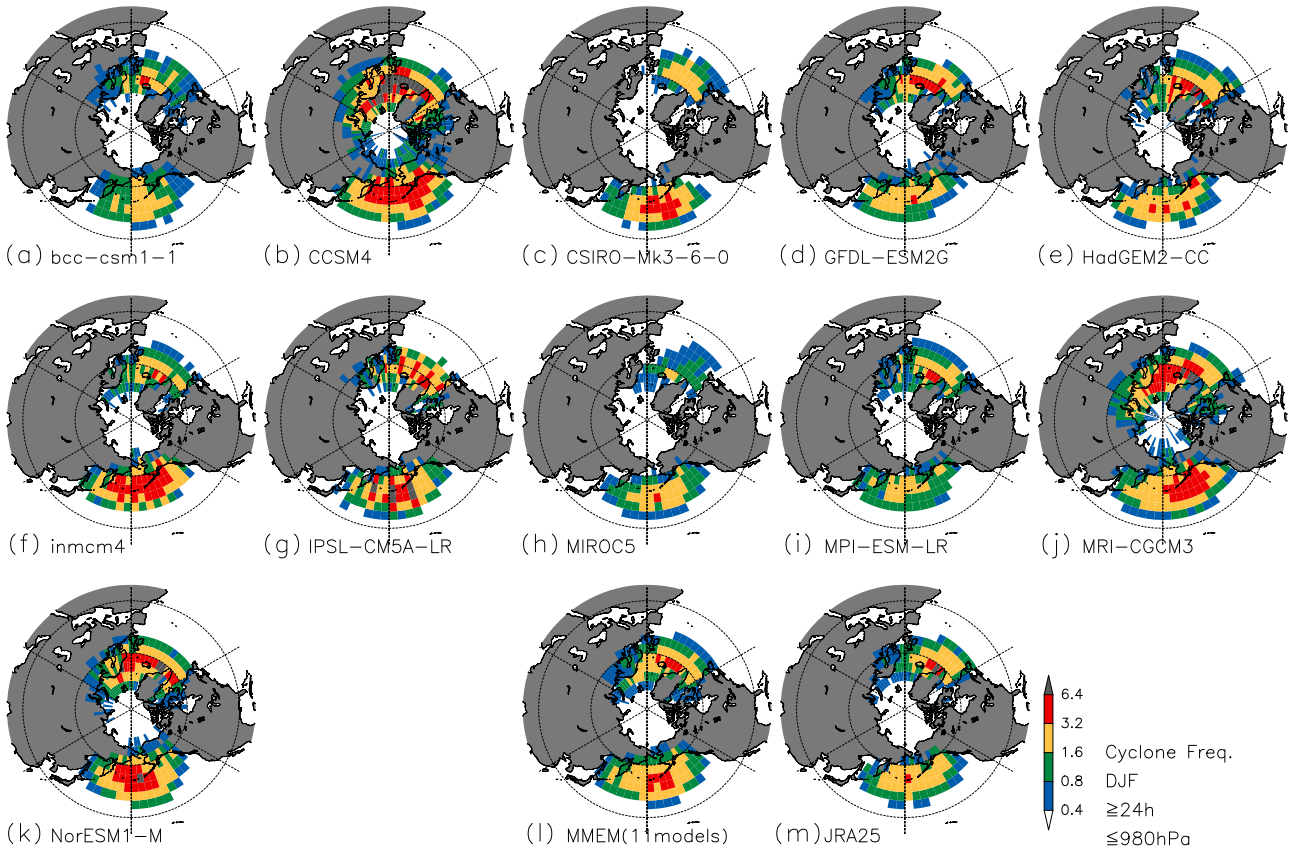

Figure 1. Density of intense cyclones, defined as the frequency of existence of cyclones that experience below 980 hPa during their lifetimes, for (a–k) the Historical run of each model, (l) the ensemble mean of all the models, and (m) the JRA-25 for the same period. It is calculated for each 5° grid box and the units are 1 per month per box.

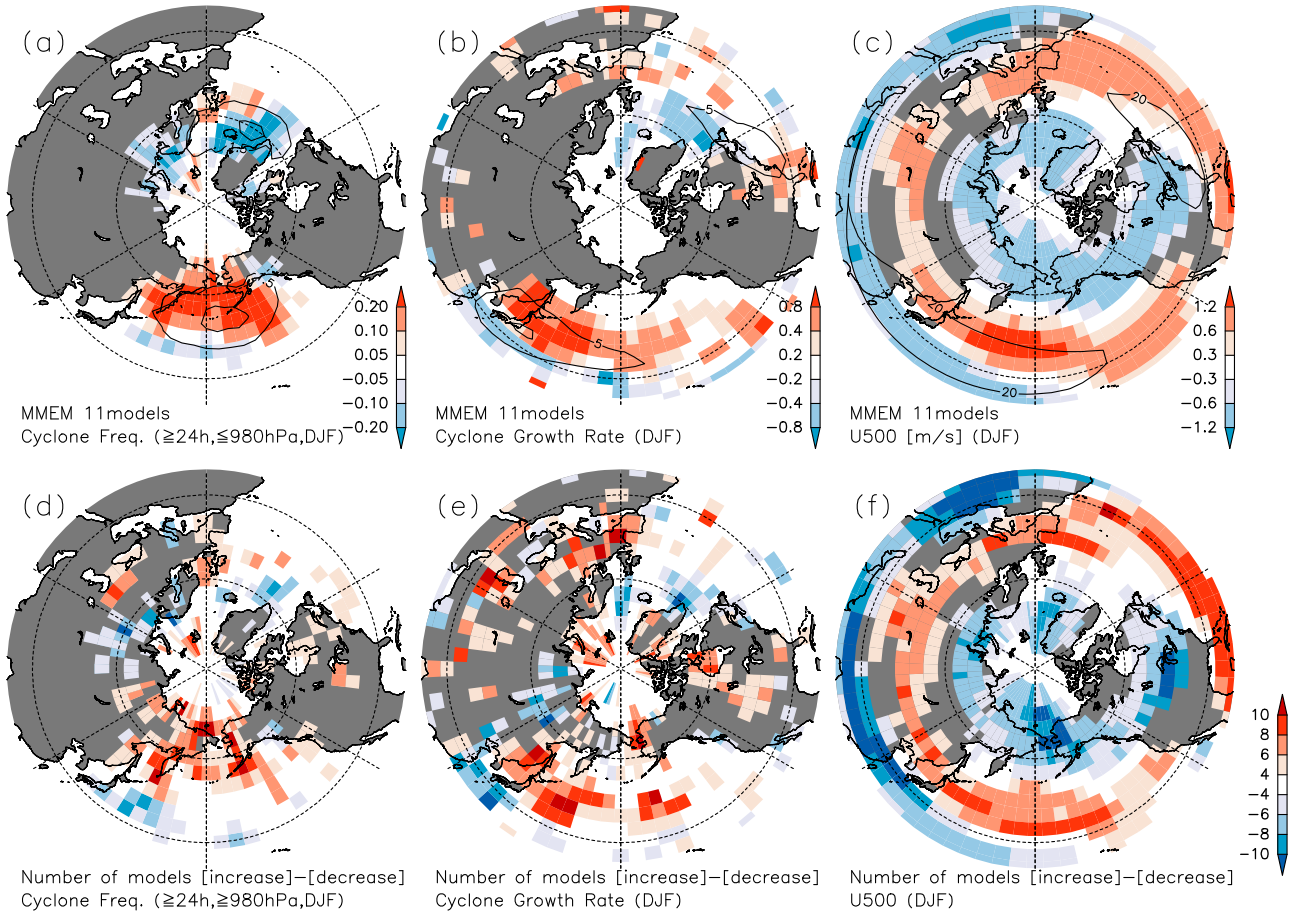

Figure 2. (top) Multi-model ensemble means of the change from the Historical runs to the RCP4.5 runs, and (bottom) the number of models that project increases minus the number of models that project decreases in (a, d) density of intense cyclones (1 per month per box), (b, e) mean growth rate of cyclones (hPa/day), and (c, f) zonal wind at 500 hPa (m/s). Contours in Figures 2a–2c denote the ensemble means of the Historical runs.

represents the number of models that project increases minus the number of models that project decreases. In this figure and hereafter, we use a 5°-mesh grid and the average over 10° × 10° region centered at each grid point is plotted.

[9] While there is a diversity among the models (see Figure S1 in the auxiliary material), a slight decrease around 40°N and an increase around 50°–60°N in the Pacific is found in the MMEM (Figure 2a).[1] The increase is located poleward of the present local maximum indicated by the contour (the same as Figure 1l). The number of models projecting an increase is large in this area, especially around 60°N (Figure 2d). In the Atlantic, while a decrease is seen from Iceland to Scandinavia, this can be affected by a small number of models having larger changes since there is less agreement in the region. The increase around the British Isles is small but is common to many of the models. The hemispheric geographical pattern of the change is consistent with *Mizuta et al.* [2011], and similar patterns are also seen in *Geng and Sugi* [2003], *Bengtsson et al.* [2006], and *Pinto et al.* [2007], using various models and various tracking methods. A similar tendency is seen in the Pacific and the Atlantic when a different definition of intense cyclones (e.g., a relative vorticity at 850 hPa exceeding 5×10^{-5} s^{-1}) is used (not shown). The seasonal precipitation is also increasing, although the total cyclone density, including weak ones, is decreasing in most of the models, consistent with *Lambert and Fyfe* [2006].

[10] The growth rate of cyclones is defined as the temporal SLP change along each cyclone track, with average values calculated for the cyclones that pass through each 10° × 10° region. In the MMEM (Figure 2b) and the agreement on the sign of the change (Figure 2e), the intensification of the growth rate is seen upstream of the regions where intense cyclones are increasing. This is also the case for each model (see Figure S1 in the auxiliary material). A large increase in the mean growth rate is clearly seen around 40°–50°N from the western Pacific to the central Pacific. All of the models agree on the increase at several points around this region. In contrast, the models agree less in the Atlantic, associated with the lower agreement on the change in intense cyclones in the region (Figure 2d). Relatively high agreement is seen in Europe and North America, while the change in the MMEM is small.

[11] As for the change in zonal wind at 500 hPa, most of the models show an intensification of the polar jet from central Asia to the central Pacific (see Figure S1 in the auxiliary material), which is also seen in the MMEM

[1]Auxiliary materials are available in the HTML. doi:10.1029/2012GL053032.

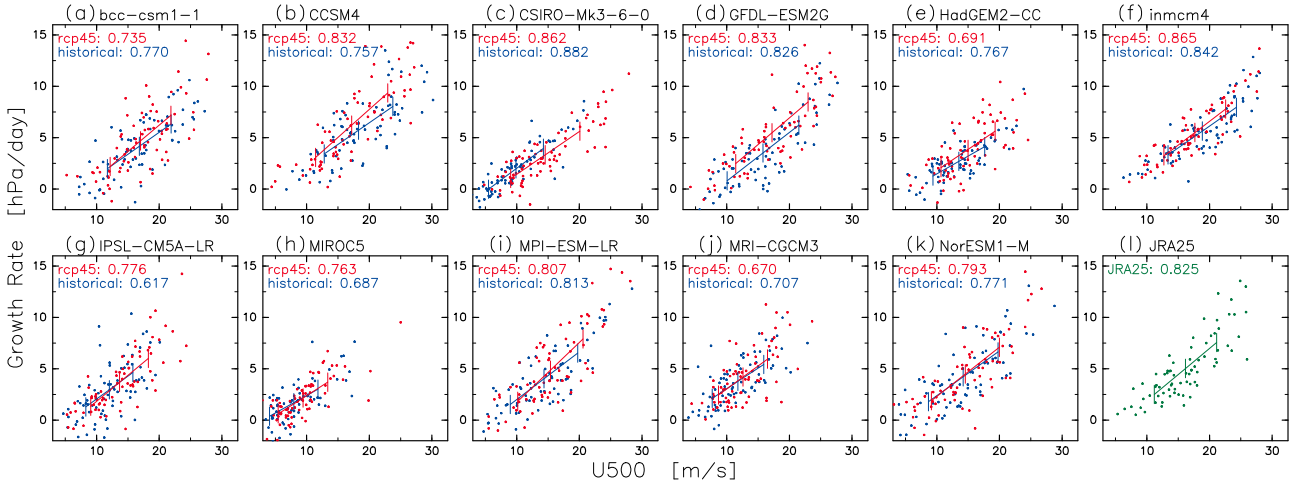

Figure 3. Scatter diagrams of the monthly-mean zonal wind at 500 hPa and the monthly-mean growth rate over 140°E–150°W, 40°N–50°N, for (a–k) the Historical run (blue) and the RCP4.5 run (red) of each model, and (l) the JRA-25 in the same period. The line denotes the regression line of the growth rate on the zonal wind. The central tick indicates the average, and the line length represents the width of the standard deviation of the zonal wind.

(Figure 2c) and the agreement on the change (Figure 2f). The agreement is very high in central Asia and the area east of Japan. The wind is also enhanced in the Atlantic but in the lower latitudes from the Gulf of Mexico to Southern Europe. The wind is weakened around 30°N from North Africa to the western Pacific. Remarkably, this geographical pattern is very similar to the pattern of the change in mean growth rate shown in Figures 2b and 2e, especially over the western Pacific and the eastern Atlantic. Note that similar patterns can be also seen in the levels from 700–300 hPa with larger changes at higher levels, and that a slight increase in the Asian subtropical jet is seen at 200 hPa in addition to the polar jet increase, meaning that the subtropical jet is shifted upward (not shown).

[12] Figure 3 presents scatter diagrams of the monthly-mean zonal wind at 500 hPa and the monthly-mean growth rate over 140°E–150°W, 40°N–50°N, where a large change exists. Each dot denotes a monthly-mean value for each of 75 months (DJF of 25 years) for each experiment. High positive correlation can be found in all of the models (Figures 3a–3k) and also in the reanalysis data (Figure 3l), consistent with the results in *Mizuta et al.* [2011]. Moreover, regression lines for the Historical run and the RCP4.5 run are close to each other. The two lines are not significantly different in 7 models when tested by analysis of covariance using a significance level of 5 percents. Therefore, the distribution is moving along the line in each model. In all but two of the models (CCSM4 and INMCM4), the long-term-mean zonal wind is increasing, and, correspondingly, the long-term-mean growth rate is increasing, without any remarkable change in the amplitude of interannual variability.

[13] Figure 4 presents the horizontal distribution of the correlation coefficient between the 500 hPa zonal wind and the monthly-mean growth rate in the JRA-25 data. The historical runs of the models show similar distributions (not shown). Although the absolute values of the correlation coefficient are smaller than those in Figure 3 since the domain size of each grid is smaller and therefore the signal-to-noise ratio is lower, positive correlation coefficients are seen over the oceans, especially high around 50°N in the western Pacific, and the western Atlantic. Although it is theoretically natural that the vertical shear over a surface baroclinic zone would facilitate the development of disturbances through baroclinic instability, the locations of high-correlation regions do not correspond to the surface baroclinic zone, represented by the high gradient of SST indicated by the contours in Figure 4.

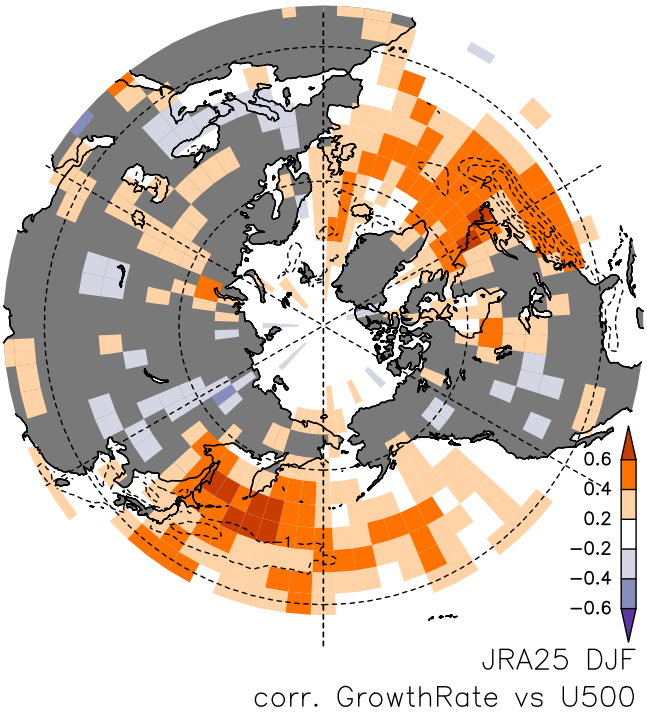

Figure 4. Local correlation coefficient between the monthly-mean zonal wind at 500 hPa and the monthly-mean growth rate in the JRA-25 data. The dotted contour denotes the meridional gradient of the climatological sea-surface temperature (interval is 1 K per degree).

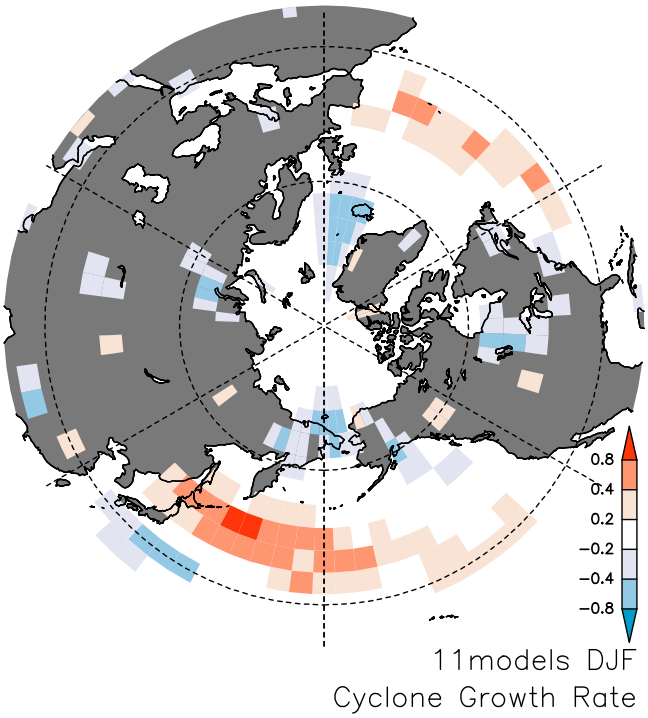

Figure 5. Change in the mean growth rate (hPa/day) estimated from the regression coefficients of the mean growth rate on the zonal wind at 500 hPa in the JRA-25 multiplied by the multi-model ensemble mean of the zonal wind change in Figure 2c.

[14] As the mean growth rate of surface cyclones is highly correlated with the mean zonal wind and the regression line does not change from the Historical run and the RCP4.5 run, we expect that the change in the mean growth rate can be estimated from only the regression coefficients of the present-day climate and the projected change in the mean zonal wind. The distribution of the regression coefficients of the mean growth rate on the zonal wind at 500 hPa in the JRA-25 reanalysis data is similar to that in Figure 4, having values around 0.3–0.6 (hPa/day)/(m/s) in the Pacific and 0.4–0.7 (hPa/day)/(m/s) in the Atlantic (not shown). Figure 5 provides the estimated change in the mean growth rate calculated from the values of the regression coefficient multiplied by the MMEM of the zonal wind change in Figure 2c at each grid. The distribution is similar to the direct calculation in Figure 2b in terms of the largest increase over 0.8 s^{-1} around 40°–50°N in the Pacific, a smaller increase around 40° in the eastern Atlantic, and a decrease in the area south of Japan and around Iceland. That is to say, the change in the mean growth rate of surface cyclones around these regions can be mostly explained by the change in long-term-mean upper-level zonal wind alone. Around the western Atlantic, however, the similarity is not so strong, suggesting there are contributions from changes other than zonal wind.

[15] Over the western Pacific, the zonal wind is enhanced in the high-correlation region, leading to a larger increase in the mean growth rate. Over the Atlantic, in contrast, changes in zonal wind in the high-correlation region differ depending on the models (Figure 2f) and close to zero in the MMEM (Figure 2c). In addition, the correlation is small in the region of enhanced zonal wind (30°–45°N in the eastern Atlantic). Therefore, the change in the growth rate in the MMEM is smaller than that in the Pacific.

4. Summary and Discussion

[16] The frequency of intense cyclones below 980 hPa is projected to increase on the polar side and downstream side of the storm tracks, and the mean growth rate of these cyclones is enhanced in areas upstream of these regions in most of the CMIP5 models, especially in the North Pacific. A high positive correlation between the monthly-mean growth rate and the monthly-mean upper-level zonal wind is seen over the ocean, both in the reanalysis and in the models. From this relationship, combined with the long-term-mean projected zonal wind change, most of the change in the mean growth rate can be estimated, without using information of cyclone trackings in the models.

[17] Over the Atlantic, the change in the growth rate is small in the multi-model ensemble mean and is highly dependent on the model used. This is associated with the low agreement of the models on the zonal wind changes over the high-correlation region. These disagreements among the models might come from disagreement in surface temperature change affected by the circulation changes in the Atlantic ocean, as pointed out by *Woollings et al.* [2012]. In contrast, over the western Pacific, the mean growth rate is enhanced in many models, associated with the intensified polar jet. The intensifications at higher latitudes facilitates overlap between the surface baroclinic zone and the mid-latitude jet, resulting in weakening of the midwinter suppression [*Nakamura*, 1992; *Nakamura and Sampe*, 2002; *Nishii et al.*, 2009] due to more frequent couplings between them. The intensified polar jet over the western Pacific can be traced back to central Asia and to Europe, suggesting that a zonal wind change leads to a change in baroclinic disturbance developments, rather than the other way around. Several mechanisms to understand the projected change in the mid-latitude jet have been proposed, such as the increase in the eddy length scale [*Kidston et al.*, 2011] and the effect of the stratospheric change [*Wu et al.*, 2012], but these have not been covered in this study. Revealing this mechanism would also contribute to reducing the uncertainty of the projection found around the North Atlantic in this study.

[18] **Acknowledgments.** We acknowledge the World Climate Research Programme's Working Group on Coupled Modeling, which is responsible for CMIP, and we thank the climate modeling groups (listed in Table 1 of this paper) for producing and making available their model output. For CMIP, the U.S. Department of Energy's Program for Climate Model Diagnosis and Intercomparison provided coordinating support and led the development of software infrastructure in partnership with the Global Organization for Earth System Science Portals. This work was supported by Grants-in-Aid for Scientific Research (23740359). The author thanks Osamu Arakawa for the data management. The GFD-DENNOU Library was used for creating the figures. We thank two anonymous reviewers for constructive comments.

[19] The Editor thanks the anonymous reviewers for assisting in the evaluation of this paper.

References

Bengtsson, L., K. I. Hodges, and E. Roeckner (2006), Storm tracks and climate change, *J. Clim.*, *19*, 3518–3543.

Geng, Q. Z., and M. Sugi (2003), Possible change of extratropical cyclone activity due to enhanced greenhouse gases and sulfate aerosols—Study with a high-resolution AGCM, *J. Clim.*, *16*, 2262–2274.

Kidston, J., G. K. Vallis, S. M. Dean, and J. A. Renwick (2011), Can the increase in the eddy length scale under global warming cause the poleward shift of the jet streams?, *J. Clim.*, *24*, 3764–3780.

Lambert, S. J., and J. C. Fyfe (2006), Changes in winter cyclone frequencies and strengths simulated in enhanced greenhouse warming experiments: Results from the models participating in the IPCC diagnostic exercise, *Clim. Dyn.*, *26*, 713–728.

Meehl, G., C. Covey, T. Delworth, M. Latif, B. McAvaney, J. Mitchell, R. Stouffer, and K. Taylor (2007), The WCRP CMIP3 multimodel dataset: A new era in climate change research, *Bull. Am. Meteorol. Soc.*, *88*, 1383–1394.

Mizuta, R., M. Matsueda, H. Endo, and S. Yukimoto (2011), Future change in extratropical cyclones associated with change in the upper troposphere, *J. Clim.*, *24*, 6456–6470.

Nakamura, H. (1992), Midwinter suppression of baroclinic wave activity in the Pacific, *J. Atmos. Sci.*, *49*, 1629–1641.

Nakamura, H., and T. Sampe (2002), Trapping of synoptic-scale disturbances into the North-Pacific subtropical jet core in midwinter, *Geophys. Res. Lett.*, *29*(16), 1761, doi:10.1029/2002GL015535.

Nishii, K., T. Miyasaka, Y. Kosaka, and H. Nakamura (2009), Reproducibility and future projection of the midwinter storm-track activity over the Far East in the CMIP3 climate models in relation to "Haru-ichiban" over Japan, *J. Meteorol. Soc. Jpn.*, *87*, 581–588.

Onogi, K., et al. (2007), The JRA-25 reanalysis, *J. Meteorol. Soc. Jpn.*, *85*, 369–432.

Pinto, J. G., U. Ulbrich, G. C. Leckebusch, T. Spangehl, M. Reyers, and S. Zacharias (2007), Changes in storm track and cyclone activity in three SRES ensemble experiments with the ECHAM5/MPIOM1 GCM, *Clim. Dyn.*, *29*, 195–210.

Taylor, K. E., R. J. Stouffer, and G. A. Meehl (2012), An overview of CMIP5 and the experiment design, *Bull. Am. Meteorol. Soc.*, *93*, 485–498, doi:10.1175/BAMS-D-11-00094.1.

Ulbrich, U., J. G. Pinto, H. Kupfer, G. C. Leckebusch, T. Spangehl, and M. Reyers (2008), Changing Northern Hemisphere storm tracks in an ensemble of IPCC climate change simulations, *J. Clim.*, *21*, 1669–1679.

Ulbrich, U., G. C. Leckebusch, and J. G. Pinto (2009), Extra-tropical cyclones in the present and future climate: A review, *Theor. Appl. Climatol.*, *96*, 117–131.

Woollings, T., J. M. Gregory, J. G. Pinto, M. Reyers, and D. J. Brayshaw (2012), Response of the North Atlantic storm track to climate change shaped by ocean-atmosphere coupling, *Nat. Geosci.*, *5*, 313–317.

Wu, Y., R. Seager, M. Ting, N. Naik, and T. A. Shaw (2012), Atmospheric circulation response to an instantaneous doubling of carbon dioxide. Part I: Model experiments and transient thermal response in the troposphere, *J. Clim.*, *25*, 2862–2879.

Yin, J. H. (2005), A consistent poleward shift of the storm tracks in simulations of 21st century climate, *Geophys. Res. Lett.*, *32*, L18701, doi:10.1029/2005GL023684.